Contrib Mineral Petrol (1998) 130: 336–345

Martin Cmíral · John D. Fitz Gerald · Ulrich H. Faul
David H. Green

A close look at dihedral angles and melt geometry in olivine-basalt aggregates: a TEM study

Received: 13 April 1997 / Accepted: 2 October 1997

Abstract Olivine-basalt aggregates sintered at high P/T have been used as a simplest approximation of partially molten upper mantle peridotite. In the past, geometry of partial melt in polycrystalline olivine (and other materials) has been characterised by dihedral (wetting) angles which depend upon surface free energy. However, since olivine (like most other crystalline materials) is distinctively anisotropic, the simple surface energy balance defining the dihedral angles $\cos(\Theta/2) = \gamma_{gb}/2\gamma_{sl}$ is not valid and melt geometry is more complicated than can be expressed by a single dihedral angle value. We examine in detail melt geometry in aggregates held at high temperature and pressure for very long times (240–612 h). We show the simple dihedral angle concept to be invalid via transmission electron microscope images. Olivine-basalt interfaces are frequently planar crystal faces (F-faces) which are controlled by the crystal structure rather than the surface area minimisation used in the simple dihedral angle concept. Nevertheless, the dihedral angles may provide useful insights in some situations. They may give a rough estimation of the wetting behaviour of a system, or be used to approximate the melt distribution if F-faces are not present (possibly at large grain size and very low melt fraction). Our measurements, excluding F-faces, give a range of dihedral angle values from 0 to 10° which is significantly lower than reported previously (20–50°). The nature of 0° angles (films and layers up to 1 μm in thickness) is unclear but their frequency compared to dry grain boundaries depends on grain size and melt fraction (e.g. 70% for grain size 43 μm and melt fraction 2%).

M. Cmíral (✉) · J.D. Fitz Gerald · U.H. Faul · D.H. Green
Research School of Earth Sciences,
Australian National University, Canberra ACT 0200, Australia
Tel: 61-2-6249 3416, fax: 61-2-6249 5989
e-mail: Martin.Cmiral@anu.edu.au

Editorial responsibility: J. Hoefs

Introduction

Some properties of partially molten material in the upper mantle are controlled by melt distribution at the scale of individual grains (Goetze 1977). For example, melt migration by porous flow will be faster if melt-filled intergranular space is well interconnected and simple in shape than if some melt remains trapped in isolated pockets (e.g. Faul 1997); seismic attenuation will increase if more melt resides in thin segregations between two grains (e.g. Schmeling 1985); and mechanical strength of mantle peridotite will be lower if more grain surfaces are wetted by melt (e.g. Hirth and Kohlstedt 1995).

Despite its importance, relatively little is known about the grain-scale melt distribution in the upper mantle. In this paper, we build on the observations of Waff and Faul (1992), by presenting an electron microscopy study of the olivine-basalt aggregates sintered at high pressure and temperature for long times. Some important details of local melt geometry are described and the significance of olivine surface energy anisotropy is stressed. Considerable emphasis is placed on the analysis of dihedral angles and discussion of their relevance in determination of melt distribution.

Theoretical background

Partially molten mantle peridotite can be viewed as an example of polycrystalline aggregates which contain a small fraction of liquid phase. Such aggregates have been extensively studied in the fields of metallurgy and ceramics (e.g. Martin and Doherty 1976; Sutton and Balluffi 1995). Theories developed to explain the behaviour of these systems predict that, at chemical equilibrium and under hydrostatic conditions, textural evolution is driven by the minimisation of total surface free energy γ, the extra free energy of atoms at interfaces

between phases and at grain boundaries[1]. Surface energy minimisation results in the interdependent processes of continuous grain growth and redistribution of liquid into lower energy configurations.

On the scale of individual grains, the problem of melt distribution reduces to the examination of the stability of an individual solid-solid grain boundary versus that of two solid-liquid interfaces. In the simplest case, the equilibrium shape of an isolated isotropic crystal is a sphere and surface energies can be expressed by vectors of surface tensions (Gibbs 1948). In a polycrystalline aggregate, the criterion for disappearance of grain boundary by wetting is: $\gamma_{gb} > 2\gamma_{sl}$, where γ_{gb} is the grain boundary energy and γ_{sl} is the solid-liquid interfacial energy. At the point of contact between grain boundary and liquid, the dihedral angle Θ is formed and is related to the surface energies by $\cos(\Theta/2) = \gamma_{gb}/2\gamma_{sl}$ (Smith 1964, p 24). In an isotropic system the dihedral angle has a unique value fully describing the geometry of liquid distribution. If $\gamma_{gb} > 2\gamma_{sl}$, $\Theta = 0^\circ$, grain boundaries are not stable and grain surfaces are completely wetted. If $0^\circ < \Theta \leq 60^\circ$, solid-solid grain boundaries are stable but melt forms an interconnected network along three- and four-grain junctions. If $\Theta > 60^\circ$, a minimum melt fraction is necessary before the melt interconnects (melt is otherwise restricted to isolated pockets at four-grain junctions).

However, the surface energy of crystalline solids is frequently anisotropic and cannot be expressed by the simple vector form of surface tensions. At equilibrium, an isolated crystal takes the form of a polyhedron whose shape depends on the relative magnitude of the surface energies of different crystal faces. The concept of an equilibrium form has been geometrically expressed by the Wulff construction (e.g. Herring 1951). Planar faces (F-faces) and sharp corners as well as smoothly curved surfaces can appear depending on the degree of anisotrophy. In a monomineralic aggregate, constraints among neighbouring growing grains prevent achievement of the complete equilibrium shape by individual crystals. Nevertheless, if a liquid is present, particular planes of the equilibrium shape may develop in contact with this liquid. The wetting criterion for a contact between two grains (I and II) must be modified to account for the orientation dependence of the surface free energies: $\gamma_{gb} > \gamma_{sl}^{I} + \gamma_{sl}^{II}$ (e.g. Kim et al. 1994). The energy of a grain boundary γ_{gb} (n,R), is a function of the surface normal n, and the misorientation between the two neighbouring crystals represented by the rotation matrix R. The energy of the solid-liquid interfaces is a function of both n and composition of the liquid phase. All surface energies depend also on temperature and pressure.

There is no simple trigonometric relationship for balancing the surface energies at triple junctions of anisotropic interfaces. The energy balance at a junction of three or more grains or phases is still poorly understood theoretically (J. Cahn, personal communication 1997) and its analysis is a very difficult problem (see for example Cahn and Kalonji, 1994 and references therein). Hoffman and Cahn (1972) and Cahn and Hoffman (1974) have modified the surface-tension method of Gibbs for isotropic surfaces and introduced a vector method for anisotropic interfaces (see also Cahn and Handwerker, 1993). It can be deduced from these works that for highly anisotropic (fully faceted) surfaces, the dihedral angle subtended between adjoining facets is not a measure of the local surface energy balance and the relationship linking such a dihedral angle to the surface energies is complex. This is also true even for less anisotropic (curved) surfaces. The simple formula $\cos(\Theta/2) = \gamma_{gb}/2\gamma_{sl}$ can be applied only if the crystalline anisotropy is negligible – i.e. at near constant curvature of the equilibrium shape.

Previous work

Returning to the materials of the Earth's upper mantle, aggregates of olivine with a few percent of basalt, sintered above solidus temperatures, have often been used as a simple experimental approximation of the partially molten upper mantle environment (see Kohlstedt, 1992 for a review). Apparent dihedral angles have been measured from scanning electron microscope (SEM) or light microscope images of melt (glass) distribution exposed on polished surfaces. The distribution of apparent angles has then been manipulated to obtain a single "true" dihedral angle (a method originally developed by Harker and Parker 1945, reviewed by Jurewicz and Jurewicz 1986) which assumes isotropic surface energy. This type of analysis has also been applied to study melt distribution in anisotropic mineral aggregates (e.g. Laporte et al. (1997). For the olivine-basalt system, dihedral angles between 20 and 50° have been reported (Waff and Bulau 1982; Riley and Kohlstedt 1991; Beeman and Kohlstedt 1993; Hirth and Kohlstedt 1995). Based on these analyses, a common view has been that the partially molten upper mantle is a relatively simple system in which melt is totally interconnected in a network of triple junction tubules where three olivine grains meet (e.g. von Bargen and Waff 1986).

Anisotropic wetting of olivine was considered by Cooper and Kohlstedt (1982) and Vaughan et al. (1982), emphasised by Bussod and Christie (1991) and more recently examined in detail by Waff and Faul (1992). The latter authors documented melt morphology deviating significantly from that of the triple junction tubule network and described the presence of F-faces as a major control on the melt distribution. Subsequently, Faul et al. (1994) showed that at melt fractions as small as 1% and grain size about 50 μm, a large proportion of melt occurs in elongated inclusions between two grain surfaces rather than in triple junction tubules. Vaughan et al. (1982) and Kohlstedt (1990) searched in detail for melt films between two grain surfaces in olivine-basalt using high resolution analytical transmission electron microscope (TEM). No thin melt films (>0.2 nm) replacing grain boundaries were found in the samples sintered at 1 GPa/1250 °C/200 hours despite predictions based on the thermodynamics of interfaces (Hess 1994) and in analogy with some ceramics (Clarke 1987), although Vaughan et al. (1982) did note 10–50 nm layers between a small fraction of grains. In the olivine-basalt system, grains completely separated by melt layers have also been reported by Jin et al. (1994) and thin films by Drury and Fitz Gerald (1996), but both are studies in deformed materials and involve strain energy factors additional to the surface energy minimisation being considered here.

[1] The term interface denotes a boundary between different phases (e.g. olivine-melt); the term grain boundary is used for a boundary between grains of the same phase

Experiments

From a set of long-duration experiments, samples that displayed steady experimental conditions (P/T) have been selected for microstructural study. The compositions of the samples and experimental details are given in Table 1 and Table 2 respectively.

The starting materials were natural olivine from mantle xenoliths collected from either Mt. Porndon in Victoria or San Carlos in Arizona, and a synthetic basalt glass. Crushed olivine grains of roughly 0.5 mm grain size were hand-picked and ground to powders. Different grain size fractions were obtained by sieving. The basalt parent mixes were prepared from high purity oxides and carbonates ground under acetone and fired at 1000 °C for 10 h. Fayalite was added prior to regrinding and melting into glass. Finally the basaltic glass was ground to fine-grained (<5 μm) powder.

Oven dried (>48 h at 200 °C) mixtures of olivine and basalt powders (up to 2 wt%) were sintered at conditions above the solidus in a 13 mm solid-media piston cylinder apparatus. The experimental temperatures were controlled using type B (Pt94/Rh6 – Pt70/Rh30) thermocouples. The experimental cell assemblies were composed of NaCl (outermost) and Pyrex glass sleeves enclosing a graphite heater, and vertical spacers made of pyrophyllite or 60% dense pure MgO. The sample capsules were made of high purity graphite sealed in Pt tube for the 1 GPa runs and Ni70/Fe30 alloy for the 0.3 GPa run[2]. Although the experiments were quenched at a rate initially exceeding 300 °C/s, it is possible that some quench growth of olivine occurred. However, we searched for characteristic quench features without success, so we conclude that the quenching has no critical effect on the microstructure (see Faul 1997 and references therein for a more detailed discussion of the quench overgrowth).

The basalt composition was based on the results of a melting experiment on Hawaiian Pyrolite (Green and Ringwood 1967) at 1200 °C and 0.3 GPa (ANU#C49/1995, unpublished data). Although originally designed for 0.3 GPa runs, this composition has been found satisfactory also for 1 GPa melt distribution experiments. At 1 GPa the basalt reacts with olivine (Jaques and Green 1980) and crystallises a minor (<1%) amount of small subhedral crystals of orthopyroxene in samples OB17, OB31 and OB32. No significant differences between composition of the pre-run and post-run olivine have been detected. Although fully quantitative analyses of the post-run basalt (glass) have not been possible because of its small volume fraction, semiquantitative analysis suggests that there is little difference between starting and post-run compositions (mainly in the Mg/Fe ratio) and that the melt retains its basaltic character in all samples.

The samples were imaged with reflected light and backscattered electrons (BSE) in a scanning electron microscope (SEM; Jeol 6400, 15 kV) to characterise the overall melt distribution. Energy dispersive spectrometry of X-rays (microprobe EDS, Oxford ISIS in Jeol 6400, 1 nA, 15 kV) was used to analyse the starting material (Table 1) as well as to check for compositional uniformity (i.e. chemical equilibrium) in the sintered aggregates. The melt fraction of the run products was visually estimated and the grain size was measured from channelling contrast BSE images (Table 2). The transmission electron microscope (TEM, Philips 430T, 300 kV) equipped with EDS (Edax) was employed for imaging the submicron-scale details of the olivine-basalt microstructure and for X-ray analysis at the scale of 10–100 nm. All micrographs (Figs. 2–4) are bright-field images. Specimens for SEM were prepared by polishing with 0.03 μm alumina powder and colloidal silica. The TEM foils were prepared by Ar-ion-milling of petrographic thin-sections.

Table 1 Composition of starting materials (EDS analysis; wt%). (*MP* olivine from Mt. Porndon, Victoria, used in OB17, OB31, OB32, *SC* olivine San Carlos, Arizona, used in SD2). Synthetic basalt (unpublished data) is a partial melt of Hawaiian pyrolite. While there is a mild reaction between the phases during the experiments, the basaltic character of the melt remains unchanged

	Olivine MP	Olivine SC	Basalt
SiO_2	41.20	40.70	51.45
TiO_2			2.50
Al_2O_3			14.36
Cr_2O_3			0.44
FeO	9.14	8.90	5.50
MnO	0.18	0.23	
NiO	0.15	0.21	
MgO	49.53	49.46	11.06
CaO			11.49
Na_2O			2.13
K_2O			0.56
Total	100.20	99.50	99.49

[2] A complementary function of the 300 MPa run was to test this capsule material for experiments in a gas-media deformation apparatus where graphite cannot be used. According to O'Neill and Wall (1987) the Ni70/Fe30 alloy is in equilibrium with mantle olivine at the upper mantle conditions

Steady-state microstructure

The purpose of the long duration of the experiments (up to 612 h) was to achieve both chemical equilibrium and a steady-state microstructure. The term steady-state microstructure is used rather than textural equilibrium since the polycrystalline aggregate at elevated temperature continues to evolve by grain growth and melt redistribution, both of which are driven by the minimisation of surface energy. However, it is assumed that by the end of all experiments the microstructure is so highly matured that dynamic effects can be neglected. From the description of compositions above, it is clear that there has been a stage early in every experiment when (bulk) chemical equilibrium is still being developed. During this early stage some transient surface morphologies may be created by rapid grain growth. However, considering diffusion coefficients on the order of 10^{-11} cm^2/s (Jurewicz and Watson 1988) relative to grain size and the long duration of our experiments, we can be confident that the chemical equilibrium is achieved (also confirmed by analyses, see above) and the transient surface morphologies are overprinted by steady-state microstructure (Waff and Faul 1992 and Faul 1997).

Melt geometry

The BSE image in Fig. 1 gives a large scale two-dimensional view of the olivine-basalt microstructure showing local melt geometry as well as most of the individual grain shapes and their relationships. This microstructure is representative of all the samples studied here and of similar materials already described in detail using SEM by Waff and Faul (1992) and Faul (1997).

From Fig. 1, it can be seen that the overall melt distribution is complicated. However, it can be viewed as

Table 2 Experimental conditions, grain sizes and melt fractions. Note particularly the long durations of the experiments

Sample	Pressure [GPa]	Temperature [°C]	Time [hours]	Initial grain size [μm]	Final mean grain size [μm]	Melt fraction [%]
OB17	1	1360	330	<25	32	1
OB31	1	1380	379	<25	34	1
OB32	1	1360	612	<25	43	2
SD2	0.3	1200	240	<10	7	1

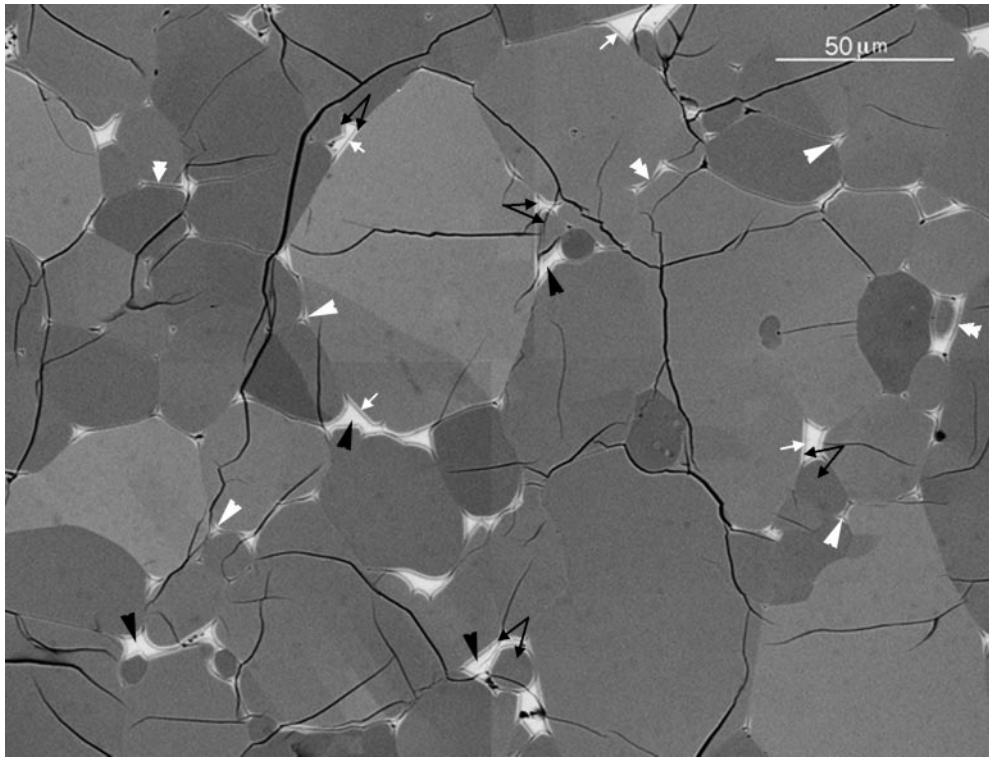

Fig. 1 BSE image showing an olivine-basalt aggregate (sample OB32) in polished section. Electron channelling produces contrast between most neighbouring crystals. This microstructure is representative of all samples studied here: Basalt glass appears *light grey*, olivine is *darker*. Melt resides mainly in large interserts (*black arrow*) and triple junctions (*white arrow*) but also in layers (*double white arrow*). Note that the large interserts are bounded by more than three grains and feature at least two non-parallel planar faces (F-faces, *small white arrows*). Where a large grain develops an F-face, there is frequently a smaller more isometric grain next to it (*black arrow pairs*). The details of triple junctions and many layers are not resolved in this BSE image. The *crosscutting black lines* are cracks formed during the quench

a spatial combination of a few types of simpler local shapes: large interserts[3], triple junctions (2D sections of triple junction tubules) and layers (or films). In the following paragraphs, we examine these individual shapes (see the summary in Table 3). All observations were carried out in TEM with the exception of large interserts which were better imaged using SEM since they are partially destroyed by ion-milling which preferentially erodes the glass phase.

Large interserts

These are of various shapes – isometric or elongated, relatively simple or very complex (Fig. 1). Their shape in 2D is defined by interfaces of more than three grains with at least two non-parallel F-faces. Frequently, at least one of the grains bordering each large intersert is distinctively smaller, and more isometric and rounded than the other grains bordering the intersert.

[3] The term intersert is derived from the classical petrographic term "intersertal texture" in which a phase (in this case, glass) occupies a volume characteristically bounded by one or more crystalline phases with euhedral faces towards the interstitial phase

Triple junctions

These are inferred to be sections through melt-filled junctions where three grains meet (triple junction tubules). Those with smoothly curved grain edges as illustrated in Fig. 2a occur only rarely. More often, the crystal surface has one or more F-faces (Fig. 2b, c) which can be smaller than 100 nm (Fig. 2d). F-faces are least developed in small triple junctions and where the three adjoining grains are large. Large F-faces are associated with triple junctions that are elongate in one direction (Fig. 2b, c). The largest inner diameter of the triple junction tubules with no F-face is about 50 nm for ~10 μm grains (SD2) and about 300 nm for ~30 μm grains (OB17). No melt-free triple junction has been found in any of the samples.

Layers

Layers of melt totally separate neighbouring grains in some places (Fig. 3a, b). They are of almost uniform thickness on the order of 10–100 nm (occasionally up to a few μm) and occur between flat as well as between

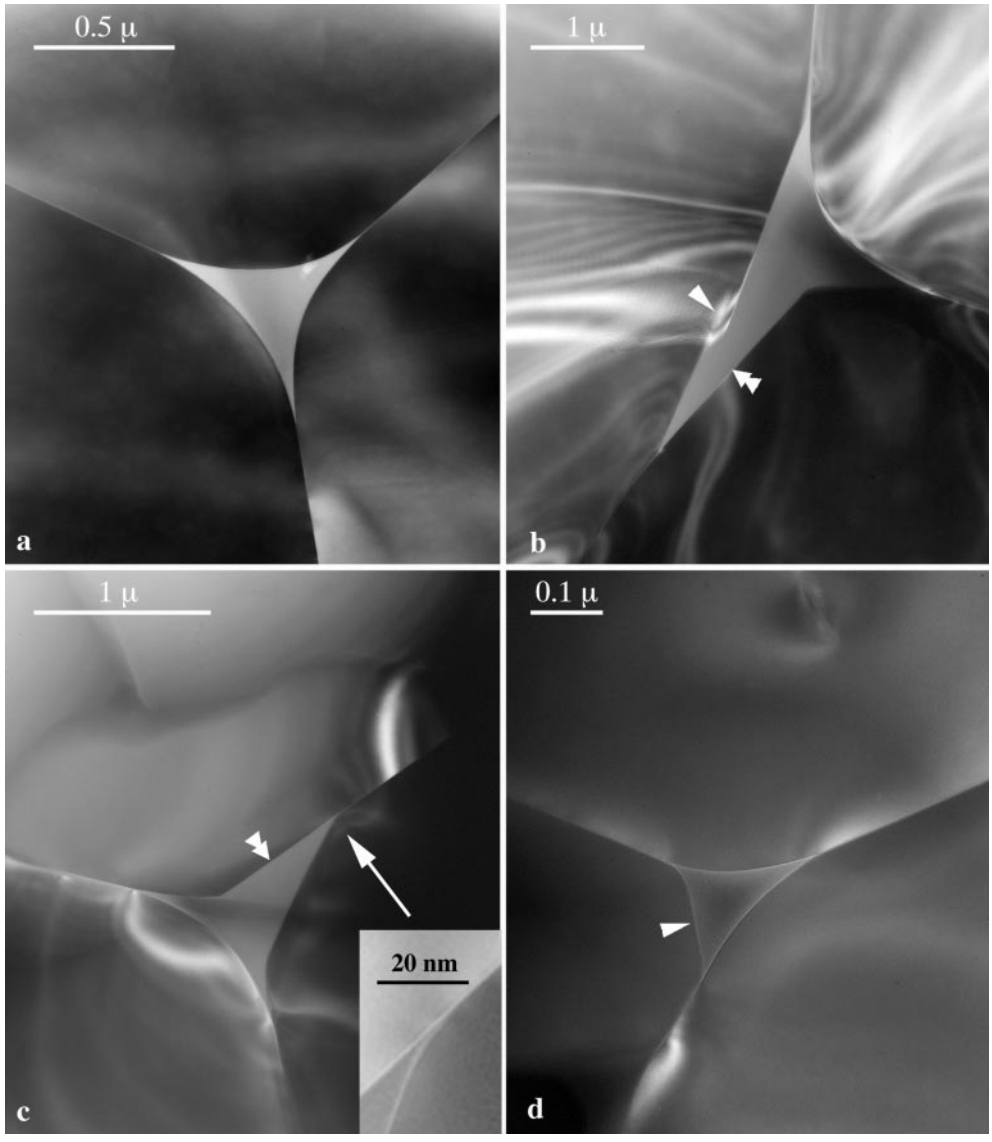

Fig. 2a–d TEM micrographs of triple junctions containing melt. Junctions are rarely as regular as in **a**. More frequently, they show one or more F-faces (**b**, **c**, **d**). In **b**, the *arrow* indicates an inclined dislocation wall terminating on F-face. The F-faces are either small, limited by curved surfaces near the grain junctions (*arrow* in **d**) or they are large and continue onto grain boundaries (*double arrows* in **b** and **c**). The trace of the F-face in **d** (*arrow*) is about 70 nm long and would not be resolved in SEM. From triple junction images like these, dihedral angles cannot be measured accurately. With the exception of **a** where all grain edges are curved, the individual junctions must be oriented even more carefully and possibly also magnified to reveal the true dihedral angle (see the *insert* in **c** and Fig. 4). In general, for a given grain size, triple junctions with F-faces (**b, c**) are larger than triple junctions without an F-face (**a**). **a**, **b**, **c** From OB17; **d** from SD2

curved grain surfaces. Layers are abundant in the sample OB32 which was sintered for the longest time and has the largest grain size. They are rare in the sample OB17 and none has been observed in the fine-grained SD2.

Films

Films with thickness on the order of 1 nm (Fig. 3c) have been detected using the X-ray analysis method of Drury and Fitz Gerald (1996). The possible orientation dependence of the layers and films as well as their frequency will be reported elsewhere (J.D. Fitz Gerald et al., and U.H. Faul and J.D. Fitz Gerald, in preparation).

The characteristics of large interserts and triple junctions indicate that the F-faces are important in controlling the local melt geometry. F-faces are low index faces typical for the olivine equilibrium shape ('t Hart 1978), however, no preferential development of the theoretically most dominant F-face (010) relative to the other equilibrium planes has been observed. Preliminary measurements in TEM suggest that the most dominant plane is (021). It is apparent that the F-faces are either small, limited by curved surfaces near the grain junctions (Fig. 2d) or by the junction itself (Fig. 4c), or they are large and continuous with grain boundaries (Fig. 2b, c). F-faces are more abundant in the fine-grained aggregates than in the coarser-grained samples (i.e. SD2 > OB17 > OB32) and better developed where the melt interserts are larger. The size of F-faces varies from a few tens of nanometres (micron sized grains in SD2; Fig. 4c) to tens of microns (grains of several tens of microns in OB32, Fig. 1). Small-scale "hill and valley" faceting which is typical for many other polycrystalline systems (Sutton and Balluffi 1995) has not been found in our experiments.

Dihedral angles

Similar in principle to the universal stage for a light microscope, the tilting capabilities of TEM (maximum tilt 60°) allow an individual grain boundary or interface (or a junction of two interfaces) in a thin foil to be oriented such that it is parallel with the electron beam within an uncertainty of about 2°, and consequently yielding an extremely narrow projected image[4]. Therefore, in principle, the individual dihedral angles at the junction between two solid-liquid interfaces can be imaged in orientations exposing their true values. In practice, we tilt one interface until it appears narrowest and check whether the other interface is acceptably narrow. By having both interfaces approximately parallel to the electron beam, we can measure the dihedral angles with an estimated error $<5°$. In many cases (e.g. Figs. 2c, 4c) it was necessary to have TEM-level resolution to image the detail of the junction.

In SEM or light microscope images of polished surfaces, there is no (3D) information to assess the inclination of individual interfaces or junctions and only apparent angles can be measured. As mentioned earlier, previous estimation of the dihedral angles for olivine-basalt was based on the calculation of a single mean value from the distribution of apparent angles by assuming random angles of junction intersections with the polished surface. This method is inherently unsuitable where, rather than a single value for an isotropic mineral, we expect a variety of dihedral angles due to crystal anisotropy.

Although time consuming, TEM with its high resolution (0.5 nm), 3D imaging and tilting capabilities provides a method to measure true dihedral angles of individual junctions albeit with $\sim 5°$ uncertainty. The results presented below (Fig. 5) show true dihedral angles that differ from those obtained by SEM for the olivinebasalt system (20–50°, reviewed by Kohlstedt, 1992).

Four categories of dihedral angles have been distinguished, with the following characteristics:

1. According to the definition of Smith (1964), the layers or films shown in Fig. 3 represent 0° dihedral angles. Preliminary observations suggest twice as many layers or films as melt-free (X-ray analysis) grain boundaries in OB32. Orientation measurements indicate that low index F-faces are not essential for the presence of layers of films.
2. Angles always smaller than 10° occur in numerous junctions where the two interfaces are either both curved or one is curved and the other is flat (examples in Fig. 4a, b). More than 50 such angles have been measured in the 4 samples. Because of the measurement inaccuracy ($\pm 5°$) we did not attempt to subdivide further dihedral angles between 0° (resolution 2 nm) and 10°. The relative proportion of these angles to the 0° angles in the samples OB32 and SD2 are about 1:2 and 1:0 respectively.
3. Large angles – 10 to 40° have been measured but these exist only between two F-faces (example in Fig. 4c). They are relatively rare in comparison with the 0–10° category – from 60 measurements only 6 large angles have been detected in the 4 samples. They are most frequent in fine-grained SD2 (30%) and least frequent in coarse-grained OB32 (10%).

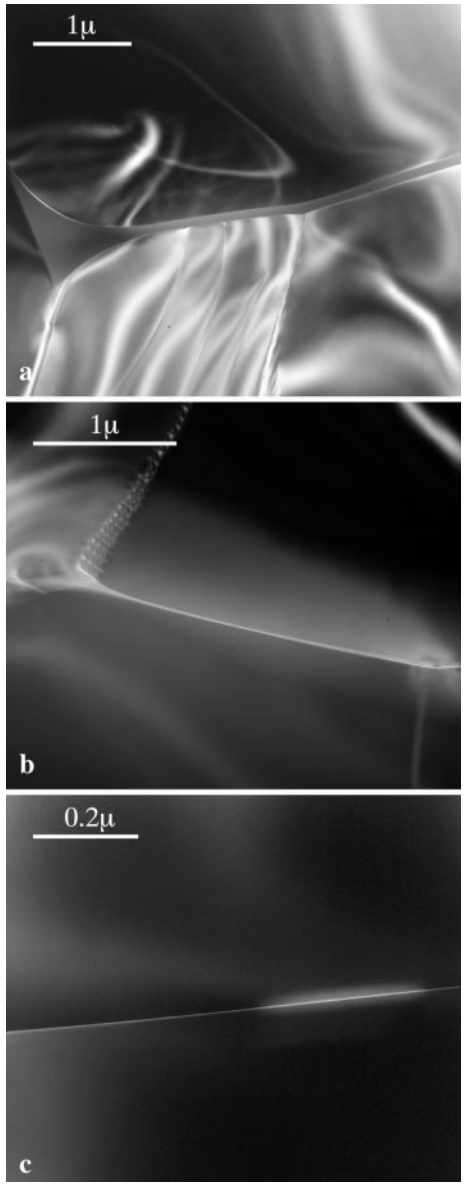

Fig. 3a–c TEM micrographs of melt layers and films: **a** a layer of 100 nm with subgrain boundaries joining one of the interfaces; **b** 20 nm layer; **c** thin film (about 1 nm) after analysing with EDS. The *light mark* results from contamination by the small elliptic electron probe used to analyse part of the grain boundary. **a** From OB32; **b**, **c** from OB31

[4] For a thick (500 nm) foil, a grain boundary or interface inclined by 1° relative to the electron beam will produce an image that is 9 nm wide, easily observable using the TEM at high magnification

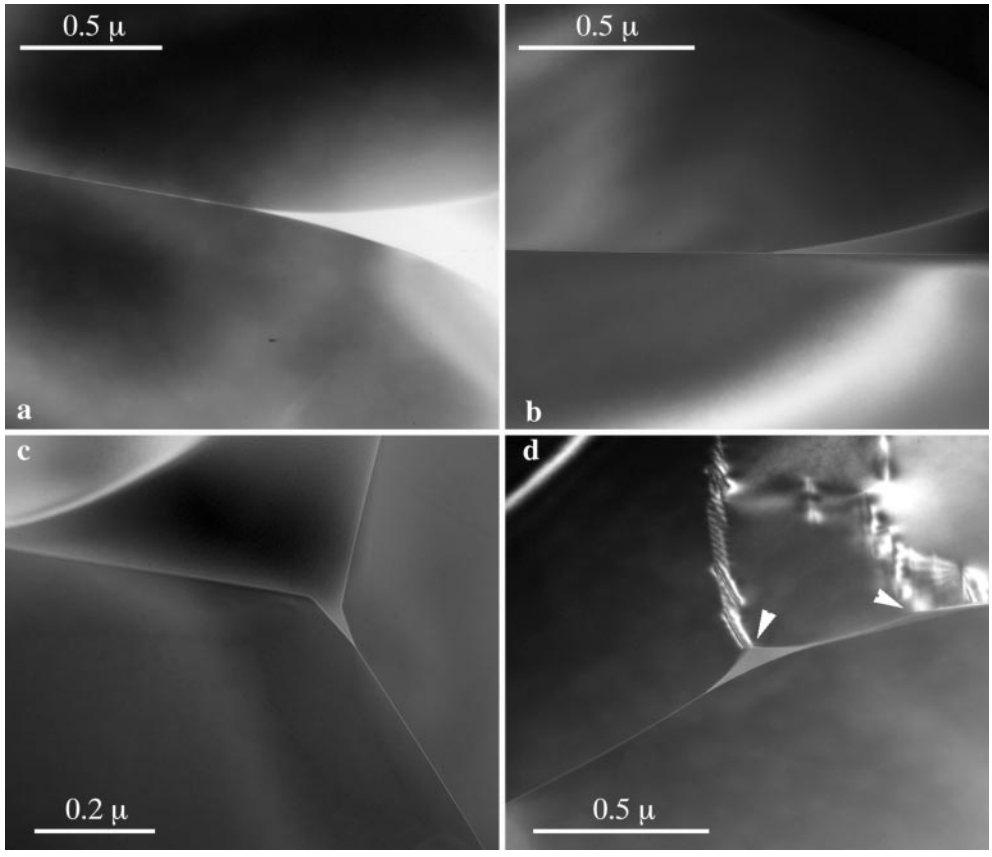

Fig. 4a–d TEM micrographs of interface junctions: **a** curved-curved, $\Theta < 10°$; **b** curved-flat, $\Theta < 10°$; **c** flat-flat, $\Theta = 20°$; **d** large angle ($\Theta > 90°$) subtended at junction with subgrain boundaries (*arrow*). **c** Shows a junction that, with resolution of conventional SEM, would have been measured as 90°. **a**, **b**, **d** From OB17; **c** from SD2

4. Very large dihedral angles (>90°) are formed where subgrain boundaries made of dislocations intersect solid-liquid interfaces (example in Fig. 4d; also see de Kloe and Drury 1997). There is one subgrain boundary per 2 grain boundaries in our samples. Fewer subgrains could be expected in nature in unstressed conditions. In the experimental samples they are produced by polygonisation of dislocations which are naturally present in the starting material and also introduced during pressurisation of the charge in the solid-media piston cylinder apparatus.

In summary, Fig. 5 shows our observations of different dihedral angle types giving an indication of their relative proportion in two aggregates of different grain sizes.

Summary and discussion

The local melt geometries in olivine-basalt aggregates observed in this study are summarised in Table 3. Whereas crystals with isotropic surface energies theoretically exist as spherical grains, anisotropic grains have exactly defined spatial relationships between crystal structure and surface shape and surface energies. F-faces are obvious structurally controlled surfaces. Their presence suggests that the microstructure does not decrease its surface free energy purely by minimisation of surface area (grain size increase) and that the melt distribution is not controlled by the simple surface free energy relationships $\cos(\Theta/2) = \gamma_{gb}/2\gamma_{sl}$. The latter is well demonstrated by the junctions between two F-faces (Fig. 4c): the dihedral angle here is the angle subtended by the two F-faces and is therefore controlled by the relative orientation of the olivine crystal axes and the Miller indices of the two F-faces but not the relative energies of the two F-faces and the grain boundary. The fact that we have measured large dihedral angles between F-faces shows directly that the relationship $\cos(\Theta/2) = \gamma_{gb}/2\gamma_{sl}$ does not apply for this configuration because it would imply that the F-faces have relatively high energy and this is very unlikely (e.g. Sunagawa 1987).

From the above it can be concluded, that wherever an F-face is present, it is the crystal structure and orientation, not surface area minimisation, that effectively control the melt distribution. This is the case in parts of all large interserts and most of the triple junctions observed in this study (see Figs. 1 and 2). Thus dihedral angles, even if their true distribution could accurately be measured with angles between two F-faces excluded, cannot sufficiently characterise the melt distribution in olivine aggregates with F-faces. This conclusion can be generalised for any partially molten polycrystalline system which develops F-faces, and argues against models where anisotropic wetting is regarded as a simple extension of the isotropic case (e.g. Laporte and Watson 1995; Hirth and Kohlstedt 1995). Our observations

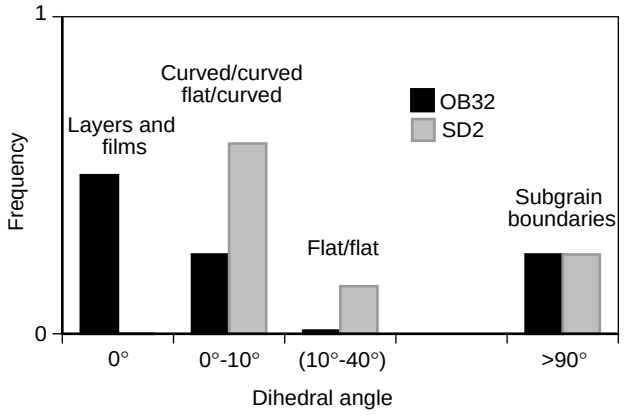

Fig. 5 Histogram showing different categories of dihedral angles in olivine-basalt aggregates. In OB32 with grain size 43 μm and melt fraction 2%, there are many layers and films but few dihedral angles in the 10–40° range; the reverse is observed for SD2 with grain size 7 μm and melt fraction 1%. This indicates that melt geometry in olivine-basalt aggregates depends on grain size and melt fraction

demonstrate that it is not possible simply to replace a single dihedral angle value in an isotropic system by a distribution of angles in an anisotropic system. A model that could theoretically describe the melt geometry in an aggregate of anisotropic crystals with F-faces at a given liquid fraction would have to take into account the proportions of F-faces of different orientation, the proportion of F-faces compared to curved interfaces and the grain size distribution.

For the sake of objectivity it should be noted here that the formation and distribution of F-faces might be somewhat different for a sintering experiment than for melting of initially solid lithologies in the mantle. For example, the large F-faces apparently continuing onto grain boundaries (Fig. 2b, c) could be an arrangement enhanced in the sintering experiments: the two grains initially grew independently and one of them developed the large F-face as a part of its equilibrium shape. During the course of sintering, the two grains came together forming a stable planar grain boundary in the orientation of the low index F-face. It is yet to be established whether grain growth (shrinking some grains and growing others) and partial melting can lead to a similar configuration.

Having argued the limitations of the dihedral angle concept, we still accept that it may provide some useful insights, for example in the following situations:

1. It is known that the development of the equilibrium crystal form is more difficult for large crystals (e.g. Herring 1951) and our experiments could reflect this since there are fewer F-faces at larger grain size. Also, the F-faces develop better where there is more liquid between crystals. Therefore, it is possible that at very large grain size and very low melt fraction, the crystallographic control is minor and the F-faces (especially the large ones which continue onto grain boundaries) cannot develop even on very long time scales. Melt distribution in such cases would be dominated by curved faces and possibly approximated by the dihedral angles in the range 0 to 10°.
2. For a rough indication of the wetting behaviour of a system, dihedral angles may be useful as long as not all surfaces are F-faces. As an example, from dihedral angle measurement it might be inferred that olivine is more

Table 3 Summary of observations. Sketches (views in section) of melt microstructures (grey) developed between olivine grains (white). Overall shapes (left) and details of individual junctions (right) are drawn

Local melt geometries	Dihedral angles
Large interserts. Shape controlled by at least two non-parallel F-faces and size differences among adjacent grains.	0° dihedral angles.
Triple junctions with F-faces. Smallest F-face about 50 nm for 10 μm grain size.	Small dihedral angles 0°-10°. Between two curved, or one flat and one curved interfaces.
Regular triple junctions. Maximum inner diameter on the order of 50 nm for 10 μm, and 300 nm for 30 μm grain size.	Large dihedral angles >10°. Between two F-faces.
Layers (10 nm to 1 μm in thickness). Films (thinner than 10 nm). At least twice as many layers as melt-free grain boundaries at 43 μm grain size. None at grain size 10 μm.	Very large angles >90°. At subgrain boundaries.

easily wet by basaltic melt than by sulphide melt (e.g. Ballhaus and Ellis 1996). In our TEM study, the small dihedral angles suggest that the wettability of olivine in the olivine-basalt system is stronger than suggested from mean angles of 20–50° measured by previous SEM studies. However, a more quantitative comparison, for example implying the degree of melt interconnectivity at a particular melt fraction will require a more complicated analysis (e.g. Faul 1997).

The circumstances under which some grains are completely separated by melt in the form of layers and films are still unclear. The presence of layers and films may depend on both melt fraction and grain size. It is unknown whether they are also a response to surface free energy minimisation (i.e. $\gamma_{gb} > \gamma_{sl}^{I} + \gamma_{sl}^{II}$) or if they are dynamic features related to grain growth. As pointed out by Hess (1994), very thin films (<2 nm) have properties (e.g. composition and viscosity) significantly different from the bulk properties of the liquid phase and should therefore be considered as a separate feature. A detailed characterisation of films and layers will be addressed in forthcoming papers (J.D. Fitz Gerald et al., U.H. Faul and J.D. Fitz Gerald, in preparation).

This study provides conclusive evidence that the melt geometry in the olivine-basalt system is more complex than the simple dihedral angle rule would dictate. The results also suggest that, even without consideration of phases additional to olivine, the direct comparison between the fine-grained experimental and coarse-grained mantle peridotite microstructures may not be straightforward. It is important to decipher the trends of the microstructure change with increasing grain size and variable melt fraction and then extrapolate them to mantle conditions.

Acknowledgements We thank Ian Jackson for comments, and Bill Hibberson, Harri Kokkonen and Andrina Norden for technical support. We are grateful to Marian Holness and Stephen Foley for critical reviews of the manuscript.

References

Ballhaus C, Ellis DJ (1996) Mobility of core melts during Earth's accretion. Earth Planet Sci Lett 143: 137–145

Beeman ML, Kohlstedt DL (1993) Deformation of fine-grained aggregates of olivine plus melt at high temperatures and pressures. J Geophys Res 98: 6443–6452

Bussod GY, Christie JM (1991) Textural development and melt topology in spinel lherzolite experimentally deformed at hypersolidus conditions. J Petrol Spec Lherzolites Issue: 17–39

Cahn JW, Handwerker CA (1993) Equilibrium geometries of anisotropic surfaces and interfaces. Mater Sci Eng A 162: 83–95

Cahn JW, Hoffman DW (1974) A vector thermodynamics for anisotropic surfaces. II. Application to curved surfaces. Acta Metall 22: 1205–1214

Cahn JW, Kalonji G (1994) Symmetries of grain boundary trijunctions. J Phys Chem Solids 55: 1017–1022

Clarke DR (1987) Grain boundaries in polycrystalline ceramics. Annu Rev Mater Sci 17: 57–74

Cooper RF, Kohlstedt DL (1982) Interfacial energies in the olivine-basalt system. In: Akimoto S, Manghnani MH (eds) High pressure research in geophysics. Adv Earth Planet Sci, pp 217–228

de Kloe R, Drury M (1997) Subgrain controlled melt topology in upper mantle rocks (abstract) EUG Abstr 9: 201

Drury MR, Fitz Gerald JD (1996) Grain boundary melt films in an experimentally deformed olivine-orthopyroxene rock: implications for melt distribution in upper mantle rocks. Geophys Res Lett 23: 701–704

Faul UH (1997) The permeability of partially molten upper mantle rocks from experiments and percolation theory. J Geophys Res 102: 10299–10311

Faul UH, Fitz Gerald JD (in preparation)

Faul UH, Toomey DR, Waff HS (1994) Intergranular basaltic melt is distributed in thin, elongated inclusions. Geophys Res Lett 21: 29–32

Fitz Gerald JD, Cmiral M, Faul UH (in preparation)

Gibbs JW (1948) Collected works, vol 1. Yale Univ Press, New Haven

Goetze CA (1977) A brief summary of our present day understanding of the effect of volatiles and partial melts on the mechanical properties of the upper mantle. In: Manghnani MH, Akimoto S (eds) High pressure research: application to geophysics. Academic Press, New York, pp 2–23

Green DH, Ringwood AE (1967) The genesis of basaltic magmas. Contrib Mineral Petrol 15: 103–190

Harker D, Parker ER (1945) Grain shape and grain growth. Trans Am Soc Met 34: 156–195

Herring C (1951) Some theorems on the free energies of crystal surfaces. Phys Rev 82: 87–93

Hess PC (1994) Thermodynamics of thin fluid films. J Geophys Res 99: 7219–7229

Hirth G, Kohlstedt DL (1995) Experimental constraints on the dynamics of the partially molten upper mantle: deformation in the diffusion creep regime. J Geophys Res 100: 1981–2001

Hoffman DW, Cahn WJ (1972) A vector thermodynamics for anisotropic surfaces. I. Fundamentals and applications to plane surface junctions. Surf Sci 31: 368–388

Jaques AL, Green DH (1980) Anhydrous melting of peridotite at 0–15 kbar pressure and the genesis of tholeiitic basalts. Contrib Mineral Petrol 73: 287–310

Jin Z-M, Green HW, Zhou Y (1994) Melt topology in partially molten mantle peridotite during ductile deformation. Nature 372: 164–167

Jurewicz SR, Jurewicz AJG (1986) Distribution of apparent angles on random sections with emphasis on dihedral angle measurements. J Geophys Res 91: 9277–9282

Jurewicz AJ, Watson EB (1988) Cations in olivine. 2. Diffusion in olivine xenocrysts, with applications to petrology and mineral physics. Contrib Mineral Petrol 99: 1109–1121

Kim D, Wiederhorn SM, Hockey BJ, Handwerker CA, Blendell E (1994) Stability and surface energies of wetted grain boundaries in aluminium oxide. J Am Ceram Soc 77: 44–53

Kohlstedt DL (1990) Chemical analysis of grain boundaries in an olivine-basalt aggregate using high resolution, analytical electron microscopy. In: Duba AG, Durham WB, Handin JW, Wang HF (eds) The brittle-ductile transition in rocks. Am Geophys Union, Washington, pp 211–218

Kohlstedt DL (1992) Structure, rheology and permeability of partially molten rocks at low melt fractions. In: Phipps Morgan J, Blackman DK, Sinton JM (eds) Mantle flow and melt generation. Am Geophys Union, Washington, pp 103–121

Laporte D, Watson BE (1995) Experimental and theoretical constraints on melt distribution in crustal sources: the effect of crystalline anisotropy on melt interconnectivity. Chem Geol 124: 161–184

Laporte D, Rapaille C, Provost A (1997) Wetting angles, equilibrium melt geometry, and permeability threshold of partially molten crustal protoliths. In: Bouchez JL, Hutton DH, Stephens WE (eds) Granite: from segregation of melt to emplacement fabrics. Kluwer, Amsterdam, pp 31–54

Martin JW, Doherty RT (1976) Stability of microstructure in metallic systems. Cambridge Univ Press, Cambridge

O'Neill HSC, Wall VJ (1987) The olivine-orthopyroxene-spinel oxygen geobarometer, the nickel precipitation curve and the

oxygen fugacity of the Earth's upper mantle. J Petrol 28: 1169–1191
Riley GN, Kohlstedt DL (1991) Kinetics of melt migration in upper mantle-type rocks. Earth Planet Sci Lett 105: 500–521
Schmeling H (1985) Numerical models on the influence of partial melt on elastic, anelastic and electrical properties of rocks. I. Elasticity and anelasticity. Phys Earth Planet Inter 41: 34–57
Smith CS (1964) Some elementary principles of polycrystalline microstructure. Met Rev 9: 1–48
Sunagawa I (1987) Morphology of crystals. Terrapub, Tokyo
Sutton AP, Balluffi RW (1995) Interfaces in crystalline materials. Oxford Univ Press, Oxford
S'Hart J (1978) The structural morphology of olivine. I. A qualitative derivation. Can Mineral 16: 175–186
Vaughan PJ, Kohlstedt DL, Waff HS (1982) Distribution of the glass phase in hot-pressed, olivine-basalt aggregates: an electron microscopy study. Contrib Mineral Petrol 81: 253–261
von Bargen N, Waff HS (1986) Permeabilities, interfacial areas and curvatures of partially molten systems: results of numerical computations of equilibrium microstructures. J Geophys Res 91: 9261–9276
Waff HS, Bulau JR (1982) Experimental determination of near-equilibrium textures in partially molten silicates at high pressures. In: Akimoto S, Manghnani MH (eds) High pressure research in geophysics. Adv Earth Planet Sci 12; pp 229–236
Waff HS, Faul UH (1992) Effects of crystalline anisotropy on fluid distribution in ultramafic partial melts. J Geophys Res 97: 9003–9014